Design and Experimental Validation of a Face-Extension Cubic Modular Robot for Shape Formation

Sumskas Karolis
Graduate School of Engineering
Kyoto University of Advanced Science
Kyoto, Japan
2024mm27@kuas.ac.jp

Hiroshi Kawakami
Graduate School of Engineering
Kyoto University of Advanced Science
Kyoto, Japan
kawakami.hiroshi@kuas.ac.jp

***Abstract*—Modular multi-robot systems capable of physical shape formation are promising for applications such as autonomous construction and reconfigurable environments. However, achieving reliable and precise assembly at small scales remains challenging due to mechanical instability and alignment uncertainty. This paper presents the design and component-level hardware validation of a 42 mm cubic modular robot based on face-extension actuation, in which modules generate motion by linearly extending faces to push and pull neighboring units. Each module integrates servo-driven X/Y actuation and passive neodymium alignment magnets. Mechanical challenges at this scale, including torsional instability, unreliable retraction, and positional errors, are addressed through a three-rod constraint system, a pin-in-channel retraction mechanism, and passive magnetic self-alignment. A centralized, constraint-aware A* planner generates cooperative action sequences that are validated in simulation and executed on physical hardware through a unified software pipeline. Experimental results on physical modules demonstrate consistent cooperative push–pull displacement (42.2 ± 0.2 mm against a 42 mm target), sub-millimeter passive alignment accuracy, and repeatable servo actuation, validating the fundamental mechanical operations required for planar shape formation. Simulation-based evaluation confirms planning scalability up to 56 modules. These results demonstrate that the key mechanical requirements for reliable small-scale modular assembly can be met through constraint-driven design without sensing or feedback-based correction.**

***Keywords*—modular robotics, multi-robot systems, shape formation, mechanical design, centralized planning**

I. Introduction

Modular multi-robot systems provide adaptable and scalable solutions for tasks requiring dynamic structural reconfiguration, with applications in autonomous construction, logistics, disaster recovery, and space exploration [1,2,3]. Among these, cubic modular systems are particularly attractive due to their geometric regularity, enabling structured grid-based planning and predictable inter-module interactions.

Prior modular robotic systems have employed diverse actuation strategies. M-Blocks [4] uses flywheel-driven momentum for reconfiguration, while M-TRAN [5] and ATRON [6] rely on rotational joints and distributed control. Crystalline [7] and TeleCubes [8] demonstrate lattice-based expansion mechanisms, and ElectroVoxel [9] employs electromagnetic pivoting for cube-based reconfiguration in both 2D and 3D. While these systems demonstrate capable physical implementations, they reflect different trade-offs between mechanical design, control architecture, and reconfiguration behavior. However, achieving precise, repeatable, sequence-driven assembly under tight positional constraints, particularly at small module scales, remains an open challenge.

This work presents the design and experimental validation of a face-extension actuation mechanism for modular cubic robots, in which modules generate motion through linear face displacement to push or pull neighboring units. In contrast to rotational or non-deterministic mechanisms, this approach enables direct, grid-aligned motion that is well-suited for sequence-based planning. Combined with centralized A*-based planning, the system produces cooperative action sequences executable without sensing, feedback, or local decision-making. The proposed system is built around a constraint-driven design philosophy, in which reliable behavior emerges from mechanical structure and precomputed action sequences rather than runtime control. This shifts system complexity away from execution and toward design-time planning and physical constraint. At the 42 mm module scale, several physical challenges arise that are not captured in simulation. Asymmetric servo loading introduces torsional instability in face panels, electromagnetic attachment alone does not ensure precise alignment, and reliable bidirectional face motion must be achieved within a compact structure. These challenges are addressed through targeted mechanical design solutions validated experimentally in this work.

The contributions of this work are as follows: (1) A face-extension actuation mechanism for planar modular robots, enabling push–pull interactions through linear face displacement. (2) A constraint-driven mechanical design that addresses torsional instability, retraction reliability, and inter-module alignment at the 42 mm scale without sensing or feedback. (3) Component-level hardware validation demonstrating servo repeatability, sub-millimeter passive alignment accuracy, and cooperative push–pull displacement consistent with grid-spacing requirements. (4) A centralized planning and execution framework with simulation-based scalability evaluation up to 56 modules.

II. System Overview

The system includes identical cubic robot modules and a four-component software stack. Each module is a self-contained 42 mm cube capable of extending a face panel on the X and Y axes to push or pull a neighboring module and engaging electromagnets on selected faces for attachment. The assembled module is shown in Fig. 1. Modules coordinate through a sequence of push and pull moves, each requiring one or more neighboring modules to act as supporters that stabilize the structure during motion. The software stack comprising a user interface, constraint-aware A* planner, command dispatcher, and 3D simulator, connects shape planning to physical execution over a unified WebSocket protocol. The software architecture is described in detail in Section IV.

Fig. 1. Assembled cubic robot module.

In the current implementation, the simulator serves as the primary platform for evaluating multi-module configurations, while physical hardware is used to validate the fundamental motion operation and mechanical behavior required for shape formation. This combined approach ensures that system-level behavior can be assessed despite limited hardware availability.

III. Physical Robot Design and Fabrication

A. Module Structure

Each robot module is a self-contained cubic unit of 42 x 42 x 42 mm size, fabricated from photopolymer resin via stereolithography (SLA) 3D printing. Resin was selected over FDM materials due to the high dimensional precision required at this scale; internal guide channels and face-panel clearances demand tolerances incompatible with typical FDM layer resolution. The module integrates two servo-driven actuation assemblies (X and Y axes), two electromagnets, mild steel discs, passive neodymium alignment magnets, an ESP32-C3 Super Mini microcontroller, a lithium battery, and a custom PCB for power distribution and wiring consolidation. The structural body is designed for modular disassembly, enabling precise assembly and maintenance of tightly integrated internal components. The compact integration of actuation, control, and power within a 42 mm module enables fully self-contained operation, which is essential for shape formation without external support or infrastructure. Exploded view is shown in Fig. 2.

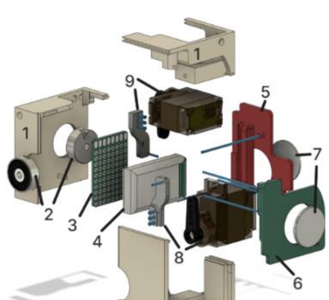

Fig. 2. Exploded view of the cubic robot module. 1 — resin structural body, 2 — electromagnets, 3 — custom PCB, 4 — lithium battery, 5 — Y-axis face panel, 6 — X-axis face panel, 7 — mild steel discs (electromagnet targets), 8 — X-axis servo assembly (motor and S-arm), 9 — Y-axis servo assembly (motor and S-arm).

B. X/Y Servo Actuation Mechanism

Each of the X and Y axes is actuated by a dedicated micro servo motor mounted inside the module body. The servo drives a custom S-shaped arm fastened directly to the servo horn. As the servo rotates, the S-shaped arm converts rotational motion into controlled linear displacement of the face panel, enabling direct push–pull interaction between adjacent modules. Unlike rotational or expansion-based actuation used in prior modular robotic systems, this mechanism enables direct linear face motion, which is fundamental to sequence-based assembly. Maximum face extension is approximately 21 mm from the module surface, or approximately 50% of the module body length. Because this extension covers only half the inter-module grid spacing, cooperative actuation from two adjacent modules is required to displace a target cube by one full grid position. This partial-displacement constraint is explicitly incorporated into the planning algorithm, ensuring that all generated motion sequences are physically executable. S-shaped arm is shown in Fig. 3.

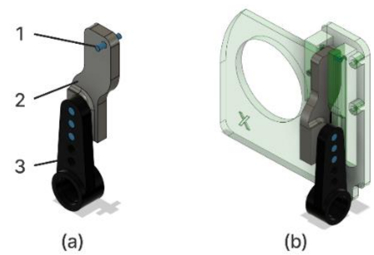

Fig. 3. S-shaped servo arm assembly. (a) Isolated arm: 1 — metal pin (1 mm diameter), 2 — S-curve arm body, 3 — servo horn attachment. (b) Arm situated within the face panel, showing spatial relationship between arm tip and face protrusions.

Retraction of the face panel is achieved through a pin-in-channel mechanism. A 1 mm diameter metal pin is press-fitted through the arm near its tip. The face panel features two parallel rectangular protrusions separated by a central gap; the arm tip passes between these protrusions during extension. As the servo rotates to its home position, the pin engages the closed end of the channel formed within the protrusions and draws the face panel flush with the module body. This mechanism achieves positive, controlled retraction under servo torque alone, without requiring a return spring, and ensures the face is fully flush with the module exterior when retracted. The face panel assembly is shown in Fig. 4.

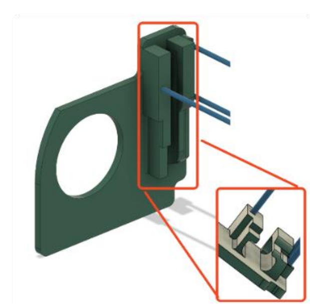

Fig. 4. Pin-in-channel retraction mechanism. The face panel protrusions form a central channel through which the S-arm tip passes during extension. On retraction, the metal pin engages the closed end of the channel, drawing the face panel flush with the module body.

A key mechanical challenge at the 42 mm scale is torsional instability during face actuation. Early prototypes show twisting of the face panel under servo load, causing binding against the module body and inconsistent extension. This was resolved by a system of three parallel 1 mm diameter stainless steel guide rods, spaced across the face panel width and running through fixed supports inside the module body. The rods constrain the face panel to pure linear translation, eliminating rotational degrees of freedom during extension and retraction. Three rods were selected to fully constrain both pitch and yaw under asymmetric loading, providing greater stability than two-rod configurations observed in early prototypes. This constraint-driven design ensures consistent actuation behavior, which is critical for maintaining execution across multi-step sequences. The internal arrangement is shown in Fig. 5.

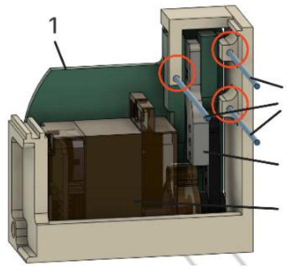

Fig. 5. Cross-section view of the X-axis actuation assembly. Guide rods (blue) run through three rod supports (highlighted by red circles), constraining the face panel to pure linear translation and eliminating torsional instability under servo load. Labels: 1 — face panel, 2 — guide rods, 3 — S-shaped arm, 4 — servo motor.

C. Inter-Module Alignment

Reliable shape formation requires precise grid alignment after each move, as positional errors can accumulate over multi-step sequences. Electromagnets alone were found insufficient for precise alignment, as their wide capture radius allows stable but misaligned connections. While alternative approaches such as Kubits [10] demonstrate that magnetic mechanisms alone can achieve connection, disconnection, and actuation without moving parts, precise positional alignment remains a challenge in purely magnetic systems. To address this, passive 3 x 1 mm neodymium disc magnets are mounted at fixed positions on the face surfaces of each module. These magnets attract and draw adjacent module faces into exact flush contact, correcting small lateral errors introduced during actuation, while remaining weak enough for the servo arm to overcome during separation. This passive alignment strategy shifts error correction from control to mechanical interaction, eliminating the need for sensing or motion-level feedback during execution. Electromagnets then provide sustained holding force throughout the sequence. Together, these mechanisms ensure that positional errors do not accumulate across multi-step sequences, enabling sub-millimeter accuracy in planar assembly. Neodymium magnet positions are shown in Fig. 6.

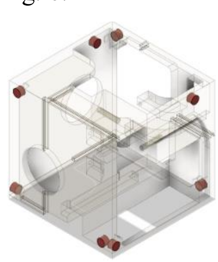

Fig. 6. Transparent view of the assembled module showing neodymium alignment magnet placement. Magnets are shown in red, embedded at fixed positions on each face surface. Eight magnets are distributed symmetrically across the X and Y faces, ensuring consistent passive alignment on all active contact faces.

IV. Unified Software Architecture

The software architecture is designed to support reliable execution by ensuring that identical command sequences can be generated, validated, and executed consistently across both simulation and physical hardware. The system consists of four main components, shown in Fig. 7: the user interface, the algorithm server, the dispatcher, and the simulator. A fifth component, the ESP32 firmware, executes commands on each module. All components communicate through a unified WebSocket-based protocol, allowing the same command sequence to be used without modification across all stages of the system pipeline.

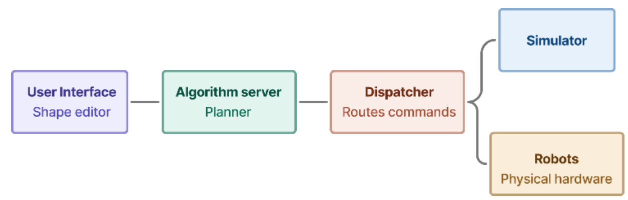

Fig. 7. Four-component software architecture connecting shape planning to simulation and physical robot execution.

A. Algorithm

The planning algorithm generates a sequence of cooperative actions that transform an initial module configuration into a target shape. It operates on a discrete 2D grid and applies a constraint-aware A* search [11], where each state represents a complete planar grid configuration and each transition corresponds to a physically valid module move.

The planner supports two cooperative move types: *push*, in which two supporter modules extend their faces in sequence to displace a target module forward by one grid position, and *pull*, in which supporters retract a target module toward them. Since each servo extends to approximately 50% of the grid spacing, both move types require two adjacent modules to actuate in sequence to complete one full displacement. At each search step, the planner iterates over all modules and all four planar directions (±X, ±Y), checking whether the target cell is empty, at least two supporters are available, no collision occurs, and the structure remains connected. Only moves satisfying all constraints are added to the search tree. The heuristic function estimates remaining cost as the sum of Manhattan distances between misplaced modules and their nearest target positions. This formulation ensures that every generated sequence is directly executable on the physical system without post-processing or runtime correction. A simulated shape formation example is shown in Fig. 8.

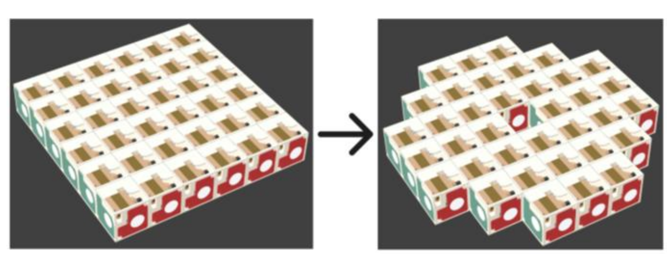

Fig. 8. Simulated shape formation example. A 6×6 planar configuration (left) is transformed into a circular ring structure (right) using a planner-generated sequence of cooperative push and pull moves.

B. Command Protocol

Commands are represented using a compact, structured format encoding using target module, action type, and execution delay. This representation ensures low communication overhead and consistent interpretation across the planning, simulation, and execution components, enabling identical command sequences to be deployed without modification.

C. Dispatcher

The dispatcher routes commands to connected modules and maintains a registry of active robots. Each connected robot is required to transmit a periodic heartbeat message every 5 seconds, robots that fail to respond within an 8-second timeout window are marked offline and excluded from dispatch. This mechanism ensures that shape formation sequences are only initiated when all required modules are confirmed active, preventing partial or inconsistent execution.

D. 3D Physics Simulator

The simulator is a custom discrete physics environment designed to efficiently evaluate multi-module interactions under the constraints of face-extension actuation. Each module is represented on a discrete grid, and motion is executed using the same command sequences as the physical system. Unlike general-purpose physics simulators, which model continuous contact and friction at high computational cost, the proposed simulator employs a simplified discrete interaction model. This enables rapid evaluation of large configurations while preserving the key constraints relevant to the system. This allows invalid or unstable sequences to be identified prior to physical execution, improving system reliability without requiring hardware testing.

E. Robot Firmware

Each robot module executes commands on an ESP32-C3 microcontroller. Incoming commands are parsed and executed, with no local decision-making or feedback-based motion correction. Servo motion is implemented using incremental position updates, allowing runtime adjustment of speed and smoothness. This design ensures consistent execution across modules while maintaining flexibility for system tuning.

V. Experiments and Results

A. Experimental Setup

Experimental validation was conducted on physical modules fabricated as described in Section III. The system was evaluated through a set of targeted experiments, each designed to isolate and characterize a specific mechanical or software subsystem. Experiments cover servo actuation repeatability, cooperative push-pull displacement, passive alignment accuracy, face retraction flush accuracy, failure mode identification, ablation of key design elements, and algorithm scalability in simulation. Hardware characterization results are summarized in Table I.

B. Servo Actuation Repeatability

Servo extension repeatability was measured by commanding each axis to full extension and recording displacement using digital calipers over 20 consecutive cycles. The X-axis produced a mean extension of 20.67 ± 0.22 mm and the Y-axis 20.76 ± 0.16 mm. A mechanical slack of approximately 1.1 mm exists in the extension range, inherent to the pin-in-channel mechanism, resulting in a total extension range of 20.4–20.5 mm. This slack is attributed to the deliberate clearance gap required for the S-shaped arm to complete the push stroke without binding against the channel walls. As passive neodymium alignment corrects lateral offsets up to 6 mm, this variance remains within the self-correction range and does not affect final positional accuracy. Command latency, measured as elapsed time between dispatcher transmission and ESP32 execution onset, averaged 32 ± 1 ms across 30 consecutive dispatches, confirming that communication overhead does not affect sequence synchronization.

C. Cooperative Push-Pull Displacement

The fundamental motion operation of the planning algorithm is a full-grid displacement of a target module, achieved through cooperative actuation from two adjacent modules. Since each servo extends to approximately 50% of the grid spacing, two sequential half-extensions are required to complete one full displacement. This was validated using a three-module configuration on both the X and Y axes. The push displacement sequence is shown in Fig. 9.

Fig. 9. Cooperative push displacement on physical hardware. Three modules in a line configuration: initial position (left), mid-displacement after two half-extensions (center), and full one-grid displacement after faces return to initial position (right). The reverse sequence performs the pull operation.

For each axis, module A extended its face to push the target module by half a grid spacing, followed by module B completing the second half. The sequence was then reversed — module B pulled the target back by half spacing, followed by module A completing the full retraction — validating both push and pull directions. Each direction was executed 10 times per axis. For push operations, total displacement was measured as the distance traveled by the target module away from the actuating pair. For pull operations, total displacement was measured as the distance traveled by the target module back toward the actuating pair, with passive magnetic alignment ensuring flush contact at the end of each pull stroke. In both cases, the target displacement is 42 mm, corresponding to one full grid spacing. Mean total displacement was 42.2 ± 0.2 mm (X-axis push, n=10), 42.0 ± 0.2 mm (X-axis pull, n=10), 42.24 ± 0.18 mm (Y-axis push, n=10), and 42.0 ± 0.2 mm (Y-axis pull, n=10). This experiment further demonstrates that the fundamental motion operation required for shape formation is physically realizable and repeatable, even with a minimal number of modules, validating the core assumption of the planning algorithm.

D. Positional Accuracy After Passive Alignment

Final module positions were measured relative to their target grid coordinates after passive self-alignment using digital calipers (resolution 0.01 mm). Mean positional error across all modules was 0.2–0.25 mm, with a maximum observed deviation of 0.38 mm across all trials. This level of accuracy is achieved without onboard sensing or feedback-based motion correction, relying primarily on mechanical constraint from the guide rod system and passive neodymium self-alignment. Importantly, positional error did not accumulate across multi-step sequences, indicating that alignment is corrected at each intermediate step rather than only at sequence completion.

E. Face Retraction Flush Accuracy

Reliable retraction to the home position is required to ensure the face panel sits flush with the module exterior between moves, preventing obstruction of neighboring modules. Retraction accuracy was evaluated over 20 full extend-retract cycles per axis, with residual offset from flush measured by digital calipers after each retraction.

The face panel retracted to a fully flush position in all 20 cycles across both axes, with zero measurable residual offset. The retracted face remained flush without play or movement, confirming that the pin-in-channel mechanism provides a consistent and rigid home position. This ensures neighboring module faces are never obstructed during operation.

F. Reliability and Failure Modes

While overall performance was consistent, three systematic failure modes were identified across trials. All were predictable and mitigable through parameter adjustment rather than requiring hardware changes.

Timing desynchronization: network latency and concurrent liveness monitoring checks occasionally introduced delays between commands, leading to partial desynchronization of robot actions. This was mitigated by increasing command delays in the sequence, with no hardware modification required.

Electromagnet sticking: in some cases, electromagnets remained connected to mild steel contact surfaces longer than the commanded disengagement time, preventing timely release. This is attributed to residual magnetization and surface contact conditions. Increasing the disengagement delay resolved the issue in all observed cases.

Premature passive alignment: neodymium magnets occasionally engaged before pull motions were fully completed, introducing additional load on the servo mechanism. This is attributed to the magnet capture radius relative to the actuation speed at the end of the pull stroke. Reducing servo speed in the final phase of retraction eliminated this failure mode.

G. Ablation Observations

To evaluate the role of key design elements, qualitative ablation observations were conducted by physically removing each component in turn and repeating the same command sequences under otherwise identical conditions. Without passive neodymium alignment magnets, modules failed to achieve proper seating after cooperative moves, resulting in cumulative positional drift that caused sequence failures within the first three moves. This confirms that passive alignment is a necessary design requirement at this scale, not an optimization. Without the three-rod constraint system, torsional deformation of the face panel under servo load caused face binding against the module body and inconsistent extension distance. Extension success rate dropped to 23% under double-rod configuration. These observations confirm that both alignment and torsion constraint are essential for reliable operation at the 42 mm scale.

TABLE I. EXPERIMENTAL RESULTS SUMMARY

Metric	Measurement	Result
Servo extension, X-axis (n=20)	Mean ± std (mm)	20.67 ± 0.22
Servo extension, Y-axis (n=20)	Mean ± std (mm)	20.76 ± 0.16
Command latency (n=30)	Mean ± std (ms)	32 ± 1
Cooperative displacement, X-axis (n=10)	Mean ± std (mm)	42.1 ± 0.2
Cooperative displacement, Y-axis (n=10)	Mean ± std (mm)	42.12 ± 0.19
Mean positional error	Mean across all modules (mm)	0.2–0.25
Face retraction flush offset	Residual offset (mm)	0 (fully flush, n=40)

H. Algorithm Scalability

The A*-based planning algorithm was evaluated across workspace sizes of 10, 20, 35, and 56 modules in simulation. For each configuration, the planner generated a complete sequence of cooperative move commands required to transform the initial state into the target shape. As summarized in Table II, the total number of move commands increases approximately linearly with workspace size, reflecting the structured nature of the planning problem. Planning time remained under 7 seconds across all tested configurations, indicating that solution generation remains computationally efficient within the evaluated range. These results suggest that planning performance is not a limiting factor in the current system, with execution constraints and mechanical stability dominating overall system scalability.

TABLE II. GENERATED COMMAND COUNTS BY WORKSPACE SIZE

Workspace size	Command amount	Planning time (s)
10 Modules	60	0.001
20 Modules	292	0.007
35 Modules	531	0.111
56 Modules	860	6.833

VI. DISCUSSION

The experimental results demonstrate that the fundamental mechanical operations required for planar shape formation at small scale can be achieved without sensing, provided that mechanical constraints and alignment mechanisms are carefully designed. Unlike many modular robotic systems that rely on feedback or decentralized coordination, the proposed approach shifts complexity from control to physical design. A key insight of this work is that mechanical constraint can effectively replace motion-level sensing in modular robotics. The combination of torsion-constrained actuation and passive magnetic alignment ensures that modules return to correct grid-aligned positions after each action, eliminating the need for runtime correction.

Due to current hardware availability constraints, full multi-module shape formation was not demonstrated physically. Instead, the system was validated through component-level experiments and simulation-based evaluation of larger configurations. The consistency between measured hardware behavior and the assumptions of the planning algorithm supports the validity of this approach.

Compared to prior cubic modular systems, the proposed approach achieves high positional precision under controlled, repeatable execution conditions. M-Blocks [4] and its 3D extension [12] reports approximately 90% success in line formation tasks using momentum-based actuation with non-deterministic interactions, with no sub-millimeter positioning accuracy reported. M-TRAN [5] and ATRON [6] rely on distributed controllers in which local decision-making introduces variability across execution instances. In contrast, the proposed system achieves a mean positional error of 0.2–0.25 mm under repeatable component-level experimental conditions, demonstrating that precise alignment can be achieved without onboard sensing. However, these comparisons reflect fundamentally different design objectives rather than equivalent benchmarks. M-Blocks optimizes for rapid, autonomous reconfiguration under uncertainty, while M-TRAN and ATRON prioritize distributed adaptability. The proposed system instead prioritizes positional precision and execution repeatability under controlled conditions, achieved through the combination of mechanical constraint and passive alignment at the cost of autonomous adaptability. The ablation results further confirm that both the guide rod constraint system and passive neodymium alignment are individually necessary for this level of performance; removing either component independently caused sequence failure within the first three moves.

The current validation is subject to several constraints that should be noted. All experiments were conducted on a flat, level surface under controlled conditions; the system does not incorporate disturbance rejection, and performance on uneven or inclined surfaces has not been evaluated. The no-sensing, open-loop approach depends on tight mechanical tolerances and consistent surface friction, variations in either could cause cumulative positioning errors over longer sequences than those tested. Communication latency (32 ± 1 ms) was stable in the current setup, but the system does not implement timeout recovery or sequence rollback in the event of missed or delayed commands, which may become relevant as module count increases and network congestion grows. Hardware availability limited physical validation to component-level and three-module cooperative experiments; behavior of the mechanical design under larger configurations, where cumulative loads, thermal effects, and inter-module tolerance stacking may emerge, remains to be validated. These limitations reflect the early-stage nature of the physical platform rather than fundamental constraints of the design approach.

Extending reliable behavior to full 3D assembly introduces additional challenges, including vertical load handling, increased coupling forces, and more complex synchronization requirements. While the hardware platform supports vertical actuation through an integrated stepper motor assembly, demonstrating the same level of precision and reliability in 3D configurations as achieved in planar assembly remains the primary open problem for this system. The centralized planning framework and constraint-driven mechanical design provide a foundation for this extension, as the same principles of mechanical constraint replacing sensing apply equally to vertical actuation.

VII. Conclusion

This paper presented a modular multi-robot system based on face-extension actuation and centralized sequence-based control, enabling the fundamental mechanisms required for precise and repeatable planar shape formation at small scale. Through a combination of constraint-driven mechanical design and passive alignment, the system achieves sub-millimeter positional accuracy without requiring sensing or feedback-based motion correction.

Component-level validation on physical hardware demonstrates consistent subsystem performance, with repeatable servo actuation and sub-millimeter passive alignment accuracy confirmed across trials. The results show that shifting complexity from control to mechanical design provides a practical alternative to sensing-driven approaches in modular robotics, while maintaining predictable and repeatable execution without onboard sensing or feedback correction.

This work establishes a foundation for constraint-driven modular robotic systems in planar assembly, demonstrating that predictable physical behavior can be achieved through the integration of mechanical design and centralized planning.

References

[1] P. Thalamy, B. Piranda, and J. Bourgeois, "A survey of autonomous self-reconfiguration methods for robot-based programmable matter," *Robot. Auton. Syst.*, vol. 120, p. 103242, 2019.

[2] M. Yim et al., “Modular Self-Reconfigurable Robot Systems,” *IEEE Robot. Autom. Mag.*, vol. 14, no. 1, pp. 43–52, 2007.

[3] G. Liang, D. Wu, Y. Tu, and T. L. Lam, "Decoding modular reconfigurable robots: A survey on mechanisms and design," *Int. J. Robot. Res.*, vol. 44, no. 5, pp. 740–767, 2025.

[4] J. W. Romanishin, K. Gilpin, and D. Rus, “M-blocks: Momentum-driven, magnetic modular robots,” in *Proc. IEEE/RSJ IROS*, 2013, pp. 4288–4295.

[5] S. Murata et al., “M-TRAN: Self-reconfigurable modular robotic system,” *IEEE/ASME Trans. Mechatronics*, vol. 7, no. 4, pp. 431–441, 2002.

[6] M. W. Jorgensen, E. H. Ostergaard, and H. H. Lund, "Modular ATRON: Modules for a self-reconfigurable robot," in *Proc. IEEE/RSJ IROS*, 2004, pp. 2068–2073.

[7] D. Rus and M. Vona, “Crystalline robots: Self-reconfiguration with compressible unit modules,” *Auton. Robots*, vol. 10, pp. 107–124, 2001.

[8] J. W. Suh, S. B. Homans, and M. Yim, "Telecubes: Mechanical design of a module for self-reconfigurable robotics," in *Proc. IEEE ICRA*, 2002, pp. 4095–4101.

[9] M. Nisser, L. Cheng, Y. Makaram, R. Suzuki, and S. Mueller, "ElectroVoxel: Electromagnetically actuated pivoting for scalable modular self-reconfigurable robots," in *Proc. IEEE ICRA*, 2022, pp. 4254–4260.

[10] S. Hauser, M. Mutlu, and A. J. Ijspeert, "Kubits: Solid-state self-reconfiguration with programmable magnets," *IEEE Robot. Autom. Lett.*, vol. 5, no. 4, pp. 6443–6450, 2020.

[11] P. E. Hart, N. J. Nilsson, and B. Raphael, “A formal basis for the heuristic determination of minimum cost paths,” *IEEE Trans. Syst. Sci. Cybern.*, vol. 4, no. 2, pp. 100–107, 1968.

[12] J. W. Romanishin, K. Gilpin, S. Claici, and D. Rus, "3D M-Blocks: Self-reconfiguring robots capable of locomotion via pivoting in three dimensions," in *Proc. IEEE ICRA*, 2015, pp. 1925–1932.